atmosphere

MDPI

*Article*

# Assessment of the Emission Characteristics of Major States in the United States using Satellite Observations of $CO_2$, CO, and $NO_2$

**Anqi Xu and Chengzhi Xiang ***

School of Remote Sensing and Geomatics Engineering, Nanjing University of Information Science and Technology, Nanjing 210044, China; 202013350080@nuist.edu.cn
* Correspondence: xcz0726@nuist.edu.cn

**Abstract:** By using space-based measurements of the column-averaged dry air mole fraction of carbon dioxide ($XCO_2$) from the Orbiting Carbon Observatory-2 (OCO-2) and CO and $NO_2$ from the Tropospheric Monitoring Instrument (TROPOMI), this study investigates the seasonal variation in the characteristics of $CO_2$, CO, and $NO_2$ across major states in the United States. Beyond correlating these trends with natural factors, significant emphasis is placed on human activities, including heating demands, energy usage, and the impacts of the COVID-19 pandemic. Concentration enhancements in observations influenced by anthropogenic emissions from urban regions relative to background values are calculated to estimate gas emissions. Our investigation reveals a strong correlation between $NO_2$ and $CO_2$ emissions, as evidenced by a correlation coefficient (r) of 0.75. Furthermore, we observe a correlation of 0.48 between $CO_2$ and CO emissions and a weaker correlation of 0.37 between CO and $NO_2$ emissions. Notably, we identify the $NO_2$ concentration as a reliable indicator of $CO_2$ emission levels, in which a 1% increase in $NO_2$ concentration corresponds to a 0.8194% ($\pm$0.0942%) rise in annual mean $CO_2$ emissions. Enhancement ratios among $NO_2$, CO, and $XCO_2$ are also calculated, uncovering that high $\Delta NO_2$: $\Delta XCO_2$ ratios often signify outdated industrial structures and production technologies, while low $\Delta$CO: $\Delta XCO_2$ ratios are linked to states that utilize clean energy sources. This approach offers a deeper understanding of the effect of human activities on atmospheric gas concentrations, paving the way for more effective environmental monitoring and policy-making.

**Keywords:** satellite observation; $CO_2$; CO; $NO_2$; emission characteristics

check for updates

**Citation:** Xu, A.; Xiang, C. Assessment of the Emission Characteristics of Major States in the United States using Satellite Observations of $CO_2$, CO, and $NO_2$. *Atmosphere* **2024**, *15*, 11. https://doi.org/10.3390/atmos15010011

Received: 22 November 2023
Revised: 17 December 2023
Accepted: 19 December 2023
Published: 21 December 2023

**Copyright:** © 2023 by the authors. Licensee MDPI, Basel, Switzerland. This article is an open access article distributed under the terms and conditions of the Creative Commons Attribution (CC BY) license (https://creativecommons.org/licenses/by/4.0/).

## 1. Introduction

In recent years, environmental issues have reached an unprecedented prominence on the global stage [1]. The IPCC's Sixth Assessment Report unequivocally articulates that the release of greenhouse gases resulting from the combustion of fossil fuels contributes to global warming and exacerbates various climate change manifestations, including extreme precipitation, prolonged heat waves, rising sea levels, permafrost thawing, and glacier and ice cap melting. The report further underscores that the rate of global warming since the 1970s has surpassed that of any previous 50-year warming interval in history [2]. Consequently, nations have grown increasingly vigilant in their efforts to monitor air quality and mitigate greenhouse gas emissions [3–5].

Carbon dioxide ($CO_2$) is the most prevalent greenhouse gas in the atmosphere and is unquestionably the most important driving factor behind climate change to date [6,7]. It not only warms the atmosphere and surface by absorbing longwave radiation from the Earth's air system and transmitting shortwave radiation from the sun but also induces supplementary continental warming through its effect on terrestrial vegetation exposed to elevated $CO_2$ concentrations [8]. $CO_2$ exhibits chemical stability and a prolonged atmospheric residence, allowing it to persist for centuries. Thus, the precise monitoring of $CO_2$ concentrations is an essential prerequisite for establishing a robust ecological environment [9–11]. Carbon monoxide (CO) is a hazardous atmospheric pollutant within the

troposphere; it can induce apnea, delayed neurological impairments, and potential fatalities in cases of elevated airborne CO concentrations that lead to CO accumulation in the human circulatory system [12]. Additionally, CO is an indirect contributor to the greenhouse effect because heightened tropospheric ozone ($O_3$) levels primarily arise from photochemical reactions associated with CO-related processes [13]. Alongside CO, nitrogen dioxide ($NO_2$) stands out as a pivotal air pollutant that presently receives paramount attention in the realm of prevention and mitigation. Increased exposure to $NO_2$ poses detrimental repercussions to human health, including but not limited to lung carcinoma [14], premature mortality [15], and asthma exacerbation [16]. Moreover, $NO_2$ acts as a precursor of $CO_2$ and $O_3$ [17,18], rendering the understanding of its spatial and temporal distribution critical for the integrated prevention and control of regional pollution. The comparison of $CO_2$ with air pollutants, such as CO and $NO_2$, offers multiple advantages in assessing urban air quality. It not only aids in distinguishing enhancements in $CO_2$ that are attributable to biological sources from those due to anthropogenic emissions but also provides insights into the distinct emission profiles of CO and $NO_2$. $CO_2$, CO, and $NO_2$, although emanating from combustion processes, have different generation mechanisms. This results in varying enhancement ratios of $\Delta CO$: $\Delta XCO_2$ and $\Delta NO_2$: $\Delta XCO_2$ that are dependent on combustion efficiency, thereby enabling the characterization of their specific emission sources. Enhancement ratios have been shown to be useful in estimating emissions from a variety of anthropogenic sources of greenhouse gases and air pollutants. Lama et al. used measurements from TROPOMI to investigate burning efficiencies in large urban centers by analyzing $NO_2$:CO enhancement ratios and comparing them to emission ratios from global inventories [19]. MacDonald et al. used space-based measurements from OCO-2/3 and TROPOMI to calculate enhancement ratios of $NO_2$, CO and $CO_2$, evaluating the validity of emissions inventories and estimating emissions from different anthropogenic sources [20]. Wan et al. utilized TROPOMI satellite data to assess large-scale emission ratios from different biomass burnings, providing insights into the relative contributions of smoldering and flaming activities in a large region and their impacts on the regional atmospheric composition and air quality [21].

The primary objective of this research is to quantify and analyze the enhancements in gas concentrations due to anthropogenic emissions and to establish a clear link between these emissions and observable atmospheric changes. We focus on understanding the interplay between various atmospheric gases and their relation to human activities, such as industrial emissions and energy consumption.

## 2. Study Area and Data

### *2.1. Study Area*

In the global context, the United States, as the sole superpower, has provided the greatest contribution to the cumulative global emissions of $CO_2$, accounting for 25% of the anthropogenic $CO_2$ accumulated in the atmosphere to date [22]. On 19 February 2021, the United States re-entered the Paris Agreement after a three-year hiatus. The commitment by President Biden to achieve net-zero emissions by 2050 is set to guide the economic and social trajectory of the United States for the forthcoming decades. This study focuses on the 10 states with the highest population in the United States (population data retrieved from https://www.census.gov/ (accessed on 20 December 2023)), areas wherein human activity is markedly intense and are indicators of anthropogenic impact [23]. According to the Energy-Related $CO_2$ Emission Data Tables from the Energy Information Administration (EIA), the $CO_2$ emissions from these states constitute 47.7% of the total U.S. emissions. This substantial share underscores the critical role that these densely populated regions play in creating the U.S.'s environmental footprint. The geographical distribution of these states in the contiguous United States is shown in Figure 1.

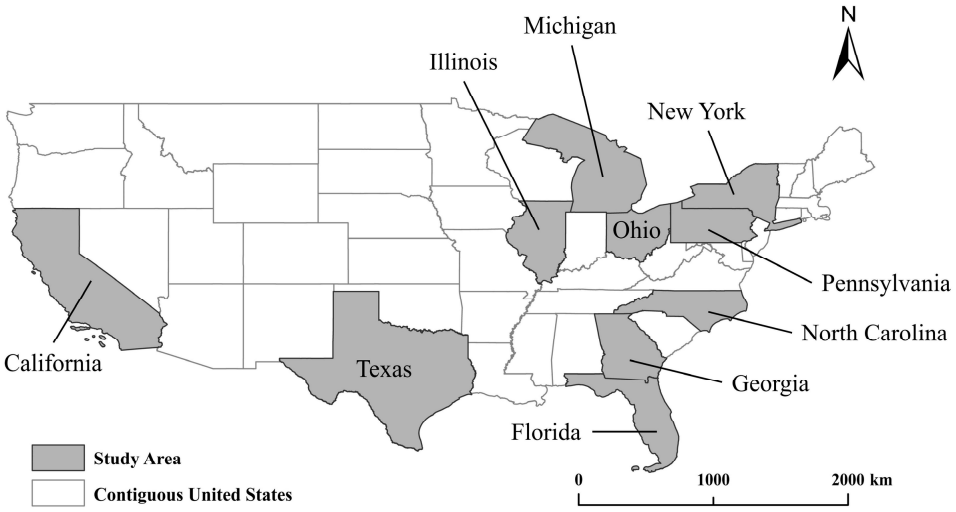


**Figure 1.** Geographical distribution of the studied states in the contiguous United States.

### *2.2. Data*

The dataset underpinning this investigation encompasses observations of $CO_2$ and $NO_2$ concentrations derived from the Tropospheric Monitoring Instrument (TROPOMI) sensor, alongside the column-averaged dry air mole fractions of $CO_2$ ($XCO_2$) retrieved through inverse modeling from the Orbiting Carbon Observatory-2 (OCO-2) satellite measurements. It is important to emphasize that the gas concentrations measured by TROPOMI are represented as total vertical columns in moles per square meter (mol/m²), whereas OCO-2 specifically quantifies $XCO_2$, which is expressed in parts per million (ppm). Principal information parameters characterizing these data are shown in Table 1.

**Table 1.** Summary of satellite data and parameters.

| Variable | Data Source | Spatiotemporal Resolution | Period |
|---|---|---|---|
| **$NO_2$** | TROPOMI sensor [24] | 1113.2 m, daily | September 2018–February 2023 |
| **CO** | TROPOMI sensor [25] | 1113.2 m, daily | September 2018–February 2023 |
| **$CO_2$** | OCO-2 satellite inversions [26] | 1.29 × 2.25 km, 16 days | September 2018–February 2023 |

#### 2.2.1. Sentinel-5 Precursor/TROPOMI

The Copernicus Sentinel-5 Precursor (Sentinel-5P), which was successfully launched on 13 October 2017 from the Plesetsk Cosmodrome in Russia, is part of the Copernicus mission dedicated to monitoring the Earth's atmosphere. The drift of trace gases and aerosols in the free troposphere has been a subject of widespread concern [27]. The primary mission of Sentinel-5P is to provide atmospheric measurements with high temporal and spatial resolutions. The satellite carries TROPOMI, which is a push-broom spectrometer designed to monitor trace gas components in the atmosphere globally [28]. TROPOMI observes the global abundance of CO by exploiting clear-sky and cloudy-sky Earth radiance measurements in the 2.3 μm spectral range of the shortwave infrared region of the solar spectrum. The TROPOMI $NO_2$ processing system is based on algorithm developments for the DOMINO-2 product and the EU QA4ECV $NO_2$ reprocessed dataset for OMI and has been adapted for TROPOMI. Sentinel-5P Level 2 products are initially categorized in a temporal sequence. The data employed herein are reprocessed on the Google Earth Engine (GEE) platform to yield gridded datasets organized by latitude and longitude coordinates. During this transformation, quality assurance (QA) filtering is applied to the source data with thresholds set on the basis of QA values: the aerosol index is filtered at a threshold of 80; the tropospheric $NO_2$ column density is set at 75%; and a general threshold of 50% is set for all other datasets, with the exception of $O_3$ and sulfur dioxide. The Level 3 products

for CO (OFF/L3_CO) and $NO_2$ (OFF/L3_$NO_2$) obtained through GEE have a resolution of 1113.2 m.

#### 2.2.2. OCO-2

OCO-2 was launched from the Vandenberg Air Force Base in California on 1 July 2014. It represents the vanguard of NASA's remote sensing satellites that were designed to collect space-based measurements of atmospheric $CO_2$. OCO-2 quantifies the intensity of the sunlight reflected from $CO_2$ present in an air column instead of measuring $CO_2$ concentrations directly. This instrument employs a diffraction grating to resolve incident solar radiation spectrally into its constituent colors to produce a detailed spectrum and measures the intensity of three relatively small wavelength bands (weak $CO_2$, strong $CO_2$, and oxygen $O_2$) from the spectrum to determine the atmospheric concentration of $CO_2$.

In the context of this study, we utilize OCO-2 Level 2 bias-corrected $XCO_2$ data, which were processed by using the version 11r retrospective algorithm. $XCO_2$ observations present a zonally striped distribution pattern. Given the sparse distribution of data points and temporal disparity within the study area, the monthly mean values for each state were computed to ascertain seasonal variation trends.

#### 2.2.3. Verification Data

We used ground-truth measurements of $NO_2$ concentrations obtained from the Environmental Protection Agency's (EPA) Air Quality System (AQS) monitoring network to verify the reliability of the satellite data. Data collection agencies report their data to the EPA via AQS, which calculates several types of aggregate (summary) data for internal use by the EPA. These data include daily and annual summaries but not monthly summaries because they are not routinely needed by the EPA. We reprocessed the data to obtain the monthly average $NO_2$ concentration for ease of validation.

#### 2.2.4. Additional Socio-Economic and Environmental Data

This study utilized socio-economic and environmental data from multiple sources. State-level forest coverage percentages were retrieved from the Wisevoter website (https://wisevoter.com (accessed on 18 October 2023)). The average winter temperatures for each state were obtained from the National Centers for Environmental Information (https://www.ncei.noaa.gov (accessed on 25 September 2023). The U.S. industrial production indices were obtained from the ycharts website (https://ycharts.com/ (accessed on 14 December 2023)). The percentage of the net electricity generated from natural gas within the borders of each state in 2021 was sourced from the Nuclear Energy Institute's website (https://www.nei.org (accessed on 18 October 2023)). The U.S.'s total traffic mileage was collected from the Bureau of Transportation Statistics (https://www.bts.gov/ (accessed on 5 December 2023)).

## 3. Accuracy Verification and Feature Analysis

### *3.1. Validation of Satellite Product Reliability*

#### 3.1.1. Sentinel-5P Product Validation

Satellite observations of atmospheric gas concentrations are commonly validated for their reliability through linear correlation analyses with ground-based empirical measurements. This study focuses on corroborating the reliability of TROPOMI sensor retrievals over the contiguous United States. To this end, $NO_2$ was chosen as a proxy pollutant. We examined eight densely populated urban centers and compared the monthly mean ground-level $NO_2$ concentrations, as measured by the AQS monitoring stations in the year 2020, with the corresponding monthly mean tropospheric $NO_2$ column densities derived from the TROPOMI sensor. Through this comparative analysis, the TROPOMI $NO_2$ column concentration data were rigorously validated against ground-truth measurements.

Figure 2 shows the correlation analysis between monthly average satellite-derived and ground-based $NO_2$ concentrations in eight cities for the year 2020. The correlation coef-

ficients for each city are as follows: Los Angeles (Pearson correlation coefficient [r] = 0.87), Washington (r = 0.95), New York (r = 0.93), Houston (r = 0.96), Philadelphia (r = 0.87), Phoenix (r = 0.87), Boston (r = 0.94), and Denver (r = 0.86). The information depicted in Figure 2 shows that the r for $NO_2$ concentrations obtained through inversion from the S5P data consistently exceeds 0.85 when compared with those of the ground-truth measurements. Consequently, this result indicates that the vertical column densities of $NO_2$ retrieved via the TROPOMI sensor are reliable.

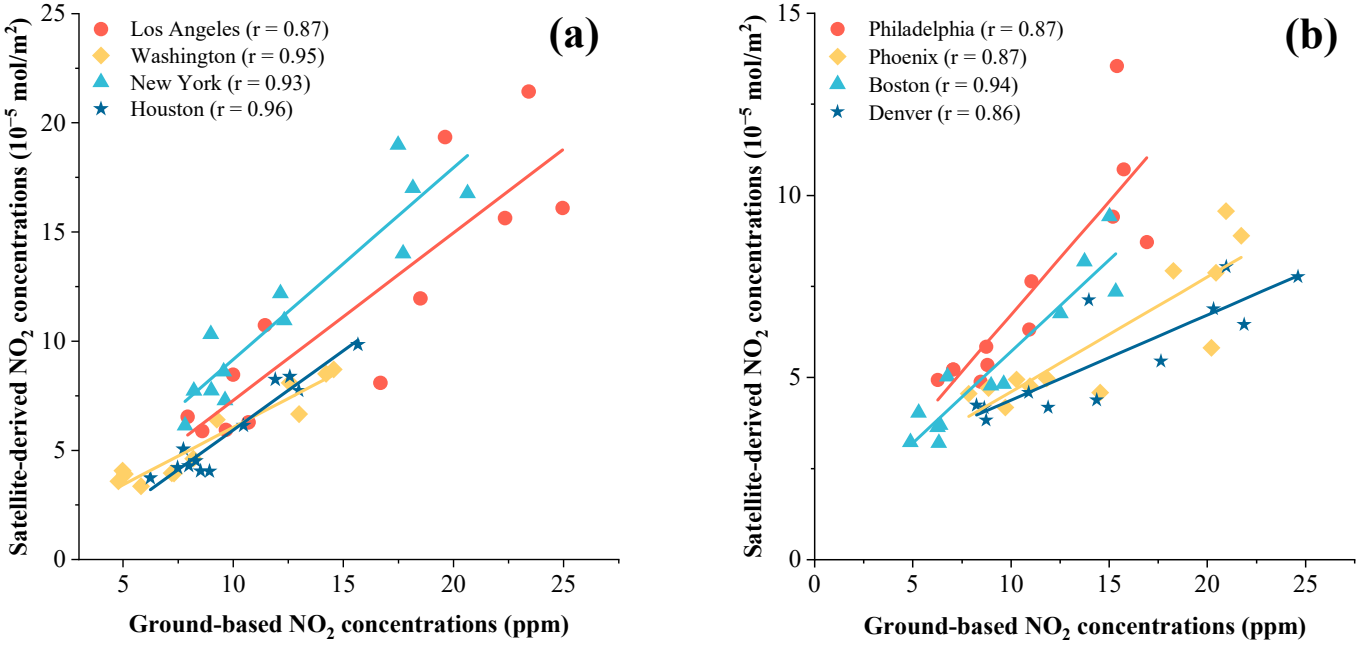


**Figure 2.** Correlations between the monthly average satellite-derived and ground-based $NO_2$ concentrations in eight cities for the year 2020. (**a**) Comparisons for Los Angeles, Washington, New York, and Houston. (**b**) Comparisons for Philadelphia, Phoenix, Boston, and Denver.

#### 3.1.2. Validation of OCO-2 Data Products

In this study, we utilized the NASA bias-corrected OCO-2 L2 Lite $XCO_2$ product version 11r. Current analyses indicate that this product exhibits an average bias of approximately 0.15 ppm when compared with the ground-based measurements from TCCON [29], demonstrating a high degree of accuracy for the dataset.

### *3.2. Analysis of $XCO_2$ Trends*

In this work, we defined seasonal intervals on an annual basis as follows: March–May for spring, June–August for summer, September–November for autumn, and December–February for winter.

Seasonal $CO_2$ concentrations within the study locale were derived from OCO-2 satellite data, as depicted in Figure 3. The line graph presents the seasonal mean $XCO_2$ trends across different states from autumn 2018 through winter 2022, illustrating the variations in $XCO_2$ levels on a state-by-state basis. Observations from 2018 onward reveal a Z-shaped ascent in $CO_2$ levels, signifying an ongoing increase that aligns with the documented mean annual rise in global $CO_2$ emissions of 1.6% post-1970 [30].

Generally, the peak annual $XCO_2$ in each state is observed during the spring season, whereas the minimum concentration is observed during the summer season. The overall pattern of $XCO_2$ exhibits a seasonal characteristic of low values in summer and autumn and high concentrations in winter and spring. Deforestation-induced land use changes and fossil fuel combustion are two factors that drastically affect atmospheric $XCO_2$ levels [31]. In spring, vegetation photosynthesis intensifies as temperatures rise. However, at this point, photosynthesis is still outweighed by soil decomposition and plant respiration, resulting in

a continued increase in $CO_2$ concentration [32]. In summer, elevated temperatures facilitate vigorous vegetative growth, which intensifies the photosynthetic processes, resulting in the augmented consumption of $CO_2$ [33]. As a result, the concentration of $XCO_2$ drops to its lowest point in summer and then rebounds in autumn. In winter, $XCO_2$ sharply rises because low temperatures lead to weakened vegetation activity and reduced $CO_2$ uptake. Additionally, the consumption of large amounts of fossil fuels for human heating contributes to the increase in $XCO_2$ in winter.

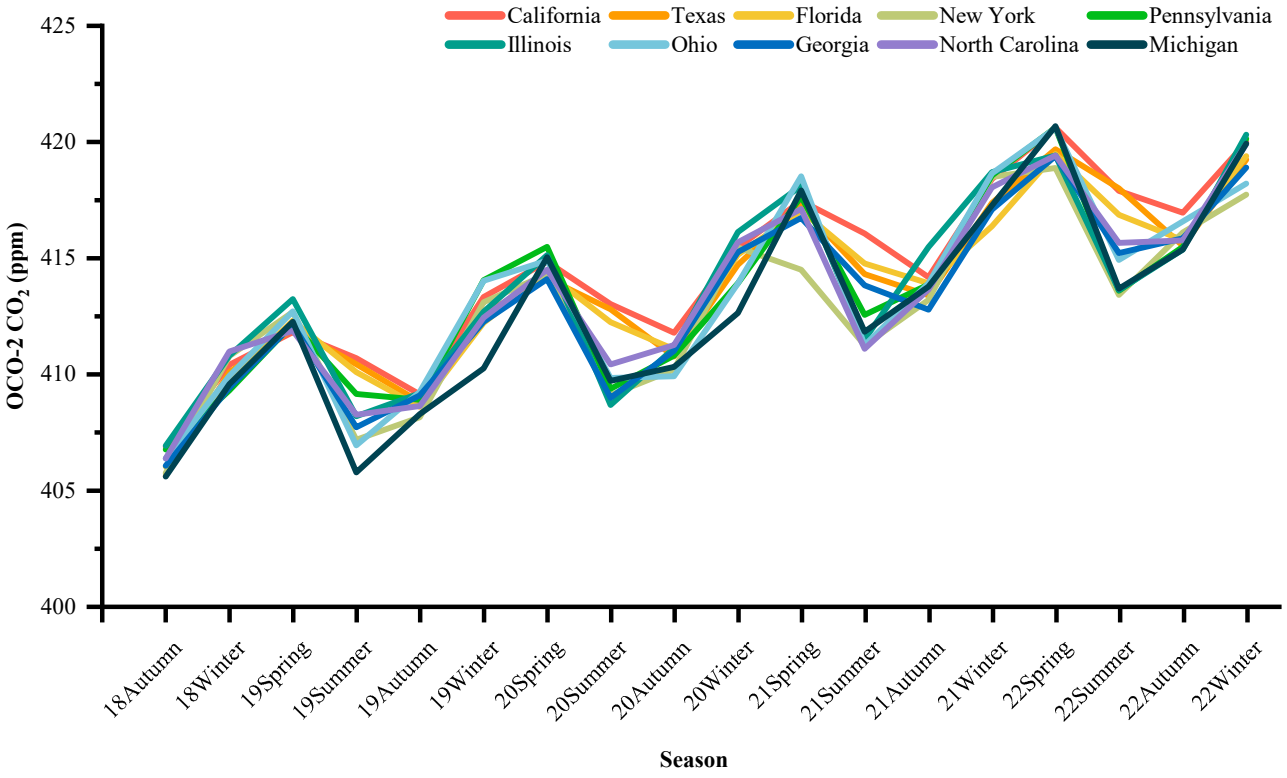


**Figure 3.** Seasonal mean $XCO_2$ trends across different states from autumn 2018–winter 2022.

The data in Table 2 delineate the incremental increases in the $CO_2$ concentration in each state in a given season relative to that in the preceding season. On the basis of the concentration growth rates presented in Table 2, during the summer months, $XCO_2$ in California, Texas, and Florida can be inferred to not exhibit a statistically significant decrease when compared with that in the other states included in the analysis. In combination with the state-by-state population and forest cover data in Table 3, we can surmise that this observation can be attributed to two primary factors. First, within the cohort, these states possess the highest population counts, which are correlated with elevated levels of energy consumption and subsequent $CO_2$ emissions. Second, these states are characterized by relatively sparse forestation. Specifically, forest coverage in California is 31.7%, whereas Texas and Florida report forest coverages of 37.1% and 49.3%, respectively, each registering below the 50% threshold. The suboptimal forest coverage in Texas and Florida results in moderate $XCO_2$ absorption during the summer months. Therefore, the seasonal amplitude in $XCO_2$ from spring to summer in these states is marginal. Although Illinois and Ohio also feature limited forest coverage, they are endowed with substantial grassland resources. Notably, Illinois, which is frequently referred to as the Prairie State, exhibits extensive grasslands that effectively sequester $CO_2$, thereby offsetting its low forestation rates [34].

**Table 2.** Incremental increases in the $CO_2$ concentration in each state in a given season relative to that in the preceding season.

| Period / State Name | 2019 | | | | 2020 | | | |
|---|---|---|---|---|---|---|---|---|
| | **Spring** | **Summer** | **Autumn** | **Winter** | **Spring** | **Summer** | **Autumn** | **Winter** |
| California | 0.34% | −0.27% | −0.38% | 1.02% | 0.37% | −0.44% | −0.30% | 0.89% |
| Texas | 0.46% | −0.37% | −0.40% | 0.93% | 0.37% | −0.32% | −0.49% | 0.96% |
| Florida | 0.63% | −0.54% | −0.36% | 0.89% | 0.52% | −0.51% | −0.28% | 0.99% |
| New York | 0.46% | −1.34% | 0.24% | 1.21% | 0.29% | −1.26% | 0.27% | 1.28% |
| Pennsylvania | 0.70% | −0.73% | −0.06% | 1.26% | 0.35% | −1.47% | 0.35% | 0.76% |
| Illinois | 0.60% | −1.22% | 0.24% | 0.86% | 0.59% | −1.56% | 0.60% | 1.22% |
| Ohio | 0.68% | −1.40% | 0.57% | 1.17% | 0.21% | −1.22% | 0.02% | 0.98% |
| Georgia | 0.67% | −1.07% | 0.34% | 0.78% | 0.45% | −1.24% | 0.49% | 1.04% |
| North Caroline | 0.22% | −0.88% | 0.09% | 0.93% | 0.50% | −0.99% | 0.20% | 1.08% |
| Michigan | 0.66% | −1.58% | 0.62% | 0.49% | 1.17% | −1.29% | 0.15% | 0.57% |
| **Period / State Name** | **2021** | | | | **2022** | | | |
| | **Spring** | **Summer** | **Autumn** | **Winter** | **Spring** | **Summer** | **Autumn** | **Winter** |
| California | 0.48% | −0.34% | −0.45% | 1.02% | 0.53% | −0.64% | −0.23% | 0.73% |
| Texas | 0.60% | −0.70% | −0.22% | 0.96% | 0.56% | −0.40% | −0.59% | 0.89% |
| Florida | 0.46% | −0.55% | −0.20% | 0.59% | 0.75% | −0.62% | −0.26% | 0.87% |
| New York | −0.23% | −0.79% | 0.48% | 1.28% | 0.10% | −1.31% | 0.65% | 0.39% |
| Pennsylvania | 0.90% | −1.22% | 0.32% | 1.14% | 0.49% | −1.68% | 0.46% | 1.12% |
| Illinois | 0.48% | −1.58% | 0.97% | 0.78% | 0.17% | −1.39% | 0.42% | 1.19% |
| Ohio | 1.12% | −1.74% | 0.65% | 1.14% | 0.47% | −1.35% | 0.40% | 0.39% |
| Georgia | 0.35% | −0.70% | −0.25% | 1.04% | 0.55% | −0.99% | 0.15% | 0.73% |
| North Caroline | 0.35% | −1.45% | 0.62% | 1.06% | 0.33% | −0.90% | 0.03% | 1.00% |
| Michigan | 1.28% | −1.46% | 0.47% | 0.85% | 0.82% | −1.67% | 0.41% | 1.10% |

**Table 3.** Population metrics and forest cover percentage by state.

| State Name | Population (Millions) | 2020 Forest Cover (%) |
|---|---|---|
| California | 39.0 | 31.7% |
| Texas | 30.5 | 37.1% |
| Florida | 22.6 | 49.3% |
| New York | 19.6 | 61.7% |
| Pennsylvania | 13.0 | 58.0% |
| Illinois | 12.5 | 13.7% |
| Ohio | 11.8 | 29.9% |
| Georgia | 11.0 | 66.5% |
| North Caroline | 10.8 | 60.3% |
| Michigan | 10.0 | 55.7% |

### *3.3. Analysis of $NO_2$ Trends*

The line graph in Figure 4 presents the seasonal mean $NO_2$ trends across different states from autumn 2018–winter 2022, illustrating the variations in $NO_2$ levels on a state-by-state basis.

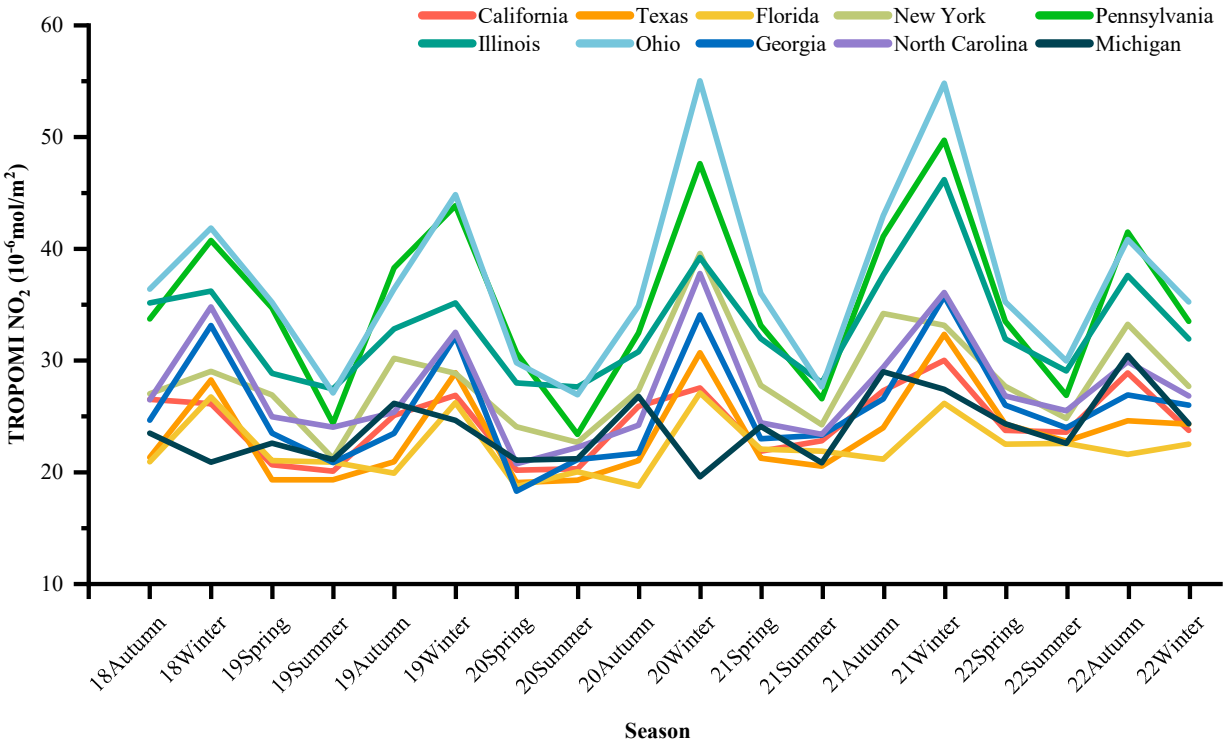


**Figure 4.** Seasonal mean $NO_2$ trends across different states during autumn 2018–winter 2022.

Between autumn 2018 and winter 2022, atmospheric $NO_2$ levels in 10 states display seasonal variations, showing high concentrations in winter and low levels in summer. $NO_2$ emissions stem from various sources, including anthropogenic, soil, and lightning emissions [35]. Additionally, meteorological conditions affect the seasonal patterns of $NO_2$ concentration [36]. In spring and summer, increased humidity and ideal diffusion conditions result in low $NO_2$ levels in the atmosphere.

In winter, $NO_2$ emissions increase and atmospheric $NO_2$ concentrations reach their peak for the year because of low temperatures and heightened heating energy usage. Based on the average winter temperatures of each state from 2018 to 2022, shown in Figure 5, we can conclude that the $NO_2$ concentration levels in Ohio, Pennsylvania, Illinois, and New York, which have low winter temperatures, are higher than those in other states such as Texas, Florida, Georgia, and North Carolina, all of which are in the southern United States, and California, which is in the western United States, because cold temperatures contribute to high heating demand. Among the 10 states, Michigan is the sole state with notably low winter temperatures and declining $NO_2$ levels during winter. One explanation for this situation could be Michigan's abundant clean energy sources. Michigan has plentiful water and wind resources due to its unique topography and climate. These resources provide ample opportunities for sustainable energy production and conservation. Furthermore, Michigan has demonstrated its ongoing commitment to promoting the use of clean energy through the implementation of Public Act 342 in 2017. This measure raised the renewable energy standard from 10% in 2015 to at least 12%. The percentage of energy produced from renewable sources increased from 5% in 2019 and 2020 to a minimum of 12.5% in 2020, with an eventual target of 15% in 2021, which is currently being achieved.

The outbreak of COVID-19 in early 2020 prompted a series of unprecedented public health responses in the United States. State-level lockdown measures were progressively implemented starting in March 2020. This period coincided with a notable decline in atmospheric $NO_2$ concentrations, as evidenced in data presented in Table 4.

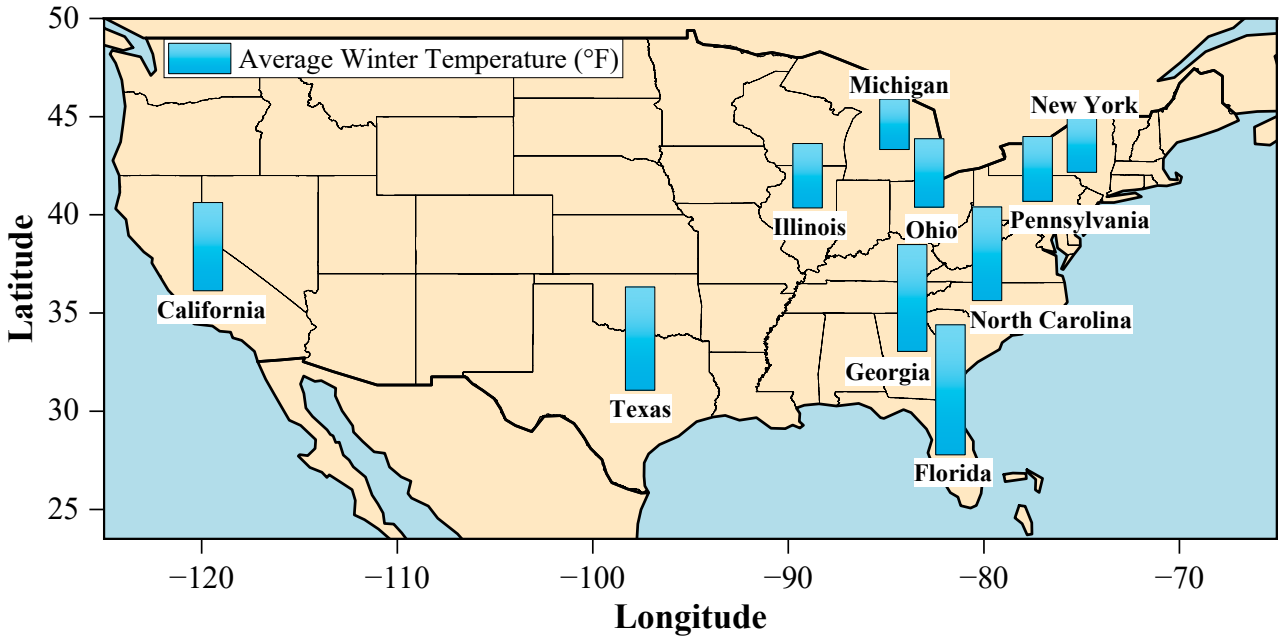


**Figure 5.** Average winter temperatures (in °F) for 10 states from 2018 to 2022.

**Table 4.** Comparison of springtime $NO_2$ concentrations (in $10^{-6}$ mol/m²) in 10 states for 2019 and 2020, with percentage increases.

| State Name | Spring 2019 $NO_2$ Concentration | Spring 2020 $NO_2$ Concentration | Increases |
|---|---|---|---|
| California | 20.59 | 20.11 | −2.37% |
| Texas | 19.26 | 19.01 | −1.27% |
| Florida | 20.99 | 18.64 | −11.19% |
| New York | 26.87 | 24.01 | −10.63% |
| Pennsylvania | 34.67 | 30.64 | −11.63% |
| Illinois | 28.81 | 27.93 | −3.05% |
| Ohio | 35.19 | 29.77 | −15.41% |
| Georgia | 23.45 | 18.23 | −22.25% |
| North Caroline | 24.90 | 20.68 | −16.93% |
| Michigan | 22.55 | 21.03 | −6.74% |

During the spring of 2020, which marked the zenith of lockdown measures, $NO_2$ concentration levels across the 10 states demonstrated reductions ranging from 1.27% to 22.25% in comparison to the corresponding period in the preceding year (spring 2019). A key factor contributing to this phenomenon is the significant downturn in industrial activities, which are a primary source of $NO_2$ emissions. The U.S. Industrial Production Index, a reliable gauge of industrial activity, remained relatively stable at around 102 throughout 2019. However, the onset of the pandemic and subsequent lockdowns led to a dramatic decrease in this index, which dropped to between 84 and 85 during the peak lockdown months of April and May 2020. This marked reduction in industrial activity, as reflected in the industrial production index, provides a cogent explanation for the observed decrease in $NO_2$ concentrations.

### *3.4. Analysis of CO Trends*

The line graph in Figure 6 presents the trends of seasonal mean CO concentrations across different states from autumn 2018–winter 2022. It illustrates the variations in CO levels on a state-by-state basis.

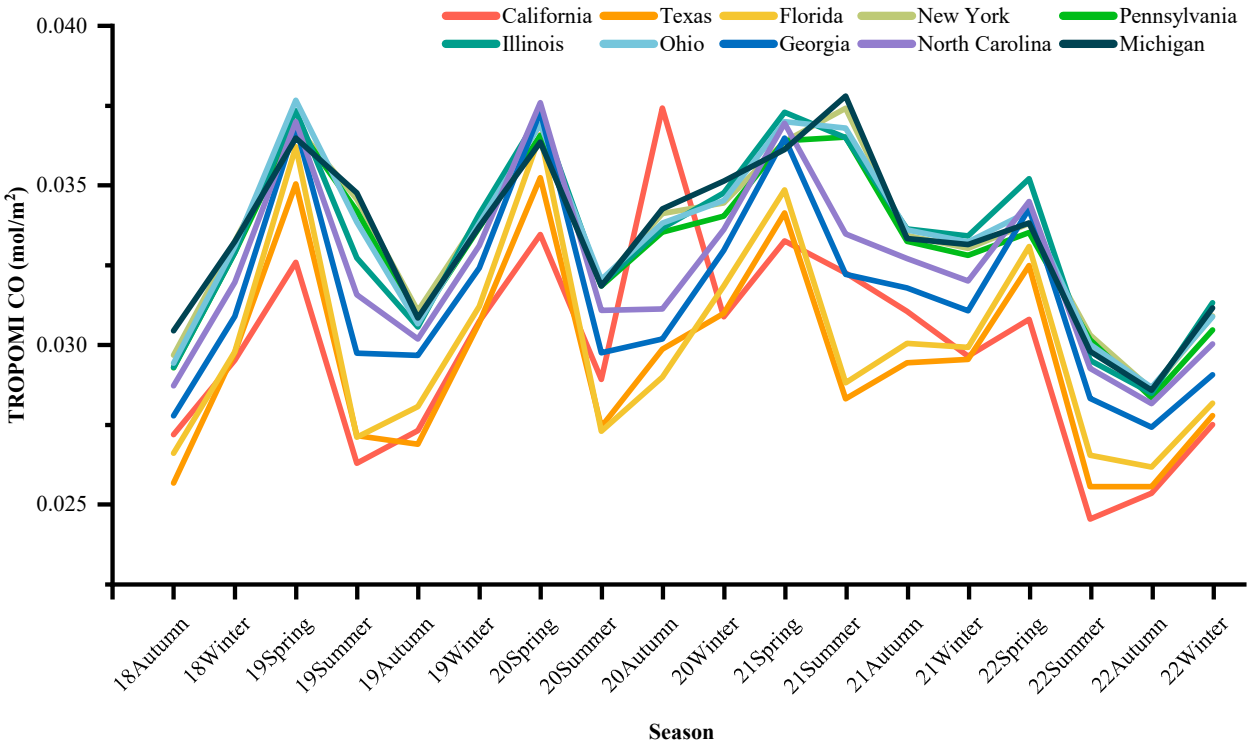


**Figure 6.** Seasonal mean CO concentration trends across different states from autumn 2018–winter 2022.

Atmospheric CO concentrations tend to have their highest values in spring and their lowest values in summer mainly because the reaction between CO and OH radicals is one of the most dominant reactions of CO, and a consistency tends to exist between the concentrations of CO emissions and OH radicals [37]. High temperatures, humidity, and strong insolation in summer are suitable for the production of OH radicals; a 30% increase in OH reduces CO production by 4–23%, and increased rainfall in summer also favors the wet deposition of gaseous pollutants [38]. During winter, when the temperature and water vapor content are low and UV radiation weakens, the low concentration of OH radicals reduces the consumption of CO. Moreover, the high-pressure control in winter is accompanied by low temperatures, resulting in the formation of an atmospheric stabilization layer that is unconducive to the diffusion of pollutants. In addition, wildfires can cause large amounts of CO to enter the atmosphere [39], causing anomalously high localized atmospheric CO concentrations. In the state of Florida during summer 2020, the anomalous CO concentrations were primarily due to the large amounts of CO emitted into the air as a result of approximately 900 hill fires. Furthermore, an examination of CO concentrations across the United States reveals a notable distinction between coastal and inland states. Coastal states such as California, Texas, Florida, Georgia, and North Carolina generally exhibit lower concentrations of CO. This difference can be largely ascribed to the unique climatic attributes inherent to coastal environments. Prevalent sea breezes, a hallmark of these areas, remarkably aid the dispersion and dilution of air pollutants, thereby mitigating the accumulation of CO. In addition, a correlation exists between the type of fuel utilized in each state and the levels of CO concentrations. This correlation is primarily driven by the degree of combustion completeness, a key determinant of CO emission levels. States in the Rust Belt region, such as Illinois, Ohio, and Michigan, exhibit consistently higher CO levels, a trend that corresponds with the region's industrial legacy and reliance on fuel types that are more susceptible to incomplete combustion. For example, while California allocated 73.9% of its electricity generation to natural gas in 2021, which is known for its low CO emissions due to high combustion completeness, Illinois only utilized 11.6% of natural gas, potentially contributing to higher CO levels.

In early 2020, the outbreak of COVID-19 prompted a series of containment strategies across states. These strategies included, but were not limited to, teleworking and traffic restrictions. According to the Bureau of Transportation Statistics (BTS), there was an 11% reduction in total traffic mileage in 2020 as compared to 2019, with only a marginal 7% recovery in 2021. Given the significant role of transportation as a major source of CO emissions, it is evident that these pandemic-related containment efforts have influenced CO concentration trends. The data presented in Table 5 illustrate the sequential seasonal increases in CO concentrations across the different states, thereby providing empirical evidence for this effect.

**Table 5.** Incremental increases in the CO concentration in each state in a given season relative to that in the preceding season.

| Period / State Name | 2019 | | | | 2020 | | | |
|---|---|---|---|---|---|---|---|---|
| | **Spring** | **Summer** | **Autumn** | **Winter** | **Spring** | **Summer** | **Autumn** | **Winter** |
| California | 10.39% | −19.35% | 3.92% | 12.53% | 8.87% | −13.59% | 29.46% | −17.50% |
| Texas | 17.80% | −22.56% | −0.98% | 14.19% | 14.80% | −22.17% | 8.88% | 3.76% |
| Florida | 21.61% | −25.17% | 3.56% | 11.17% | 17.27% | −25.44% | 6.25% | 9.88% |
| New York | 10.91% | −6.26% | −10.14% | 9.42% | 6.93% | −12.17% | 6.89% | 1.00% |
| Pennsylvania | 12.19% | −7.32% | −10.10% | 9.52% | 8.60% | −12.93% | 5.31% | 1.49% |
| Illinois | 13.50% | −12.37% | −6.63% | 11.58% | 9.27% | −14.40% | 5.55% | 3.29% |
| Ohio | 13.86% | −10.17% | −9.40% | 10.27% | 9.19% | −13.19% | 5.53% | 2.10% |
| Georgia | 19.36% | −19.35% | −0.25% | 9.27% | 15.14% | −20.26% | 1.43% | 9.25% |
| North Caroline | 15.78% | −14.68% | −4.41% | 9.72% | 13.55% | −17.34% | 0.13% | 8.02% |
| Michigan | 9.78% | −4.72% | −11.30% | 9.32% | 7.84% | −12.43% | 7.63% | 2.52% |
| **Period / State Name** | **2021** | | | | **2022** | | | |
| | **Spring** | **Summer** | **Autumn** | **Winter** | **Spring** | **Summer** | **Autumn** | **Winter** |
| California | 7.70% | −3.02% | −3.75% | −4.50% | 3.88% | −20.37% | 3.30% | 8.54% |
| Texas | 10.20% | −17.11% | 4.01% | 0.33% | 9.98% | −21.36% | 0.00% | 8.72% |
| Florida | 9.48% | −17.38% | 4.28% | −0.43% | 10.59% | −19.80% | −1.36% | 7.62% |
| New York | 5.58% | 2.85% | −10.65% | −1.19% | 2.32% | −10.35% | −5.62% | 8.06% |
| Pennsylvania | 6.98% | 0.32% | −8.95% | −1.34% | 2.19% | −10.06% | −6.03% | 7.49% |
| Illinois | 7.26% | −2.12% | −7.85% | −0.64% | 5.34% | −16.18% | −3.51% | 10.00% |
| Ohio | 7.16% | −0.52% | −8.70% | −1.13% | 2.89% | −12.21% | −4.49% | 7.73% |
| Georgia | 10.68% | −11.71% | −1.35% | −2.23% | 10.30% | −17.41% | −3.17% | 6.01% |
| North Caroline | 9.92% | −9.38% | −2.34% | −2.13% | 7.77% | −15.18% | −3.75% | 6.62% |
| Michigan | 2.84% | 4.64% | −11.84% | −0.55% | 2.05% | −11.93% | −4.08% | 9.03% |

Following the emergence of COVID-19, CO concentrations exhibited a stabilization and an overall decline. This trend was particularly noticeable during winter, a period typically less influenced by natural factors. Notably, the winter of 2020 saw a deceleration in the rise of CO levels, and in the subsequent winter of 2021, a more pronounced downward trajectory was observed in most states, deviating from the usual winter patterns in CO concentration. This deviation returned to more typical patterns in 2022, concurrent with the easing of COVID-19, although the increase in CO levels remained marginally lower than those recorded in 2019. It is important to consider the delayed atmospheric response to the preventive and control measures initiated around March 2020. This delay can be attributed to two primary factors: the time required for the implementation of these policies and the

time needed for the atmospheric assimilation of the accumulated CO. Consequently, there is an inherent lag in the response of CO concentrations to reductions in emissions.

## 4. Synergistic Analysis

Our study aims to estimate the variations in CO, $CO_2$, and $NO_2$ concentrations attributable to human activities across various states. The short life span of $NO_2$ allows us to use the observed concentration as an estimate of $NO_2$ emissions. The estimated $NO_2$ emission is denoted as $\Delta NO_2$, and the value of $\Delta NO_2$ is numerically equivalent to the concentration of $NO_2$. It should be emphasized that while this equivalence is valid within the scope of this study, the dynamics of $NO_2$ in the atmosphere are in fact more intricate. The atmospheric concentration of $NO_2$ is not solely determined by anthropogenic emissions. Natural sources, such as lightning and soil emissions, along with significant sinks including atmospheric chemical reactions and photolysis, also play a crucial role. Given the long atmospheric lifetimes of CO and $CO_2$, concentrations measured by observational instruments do not precisely reflect emission levels. A background for CO and $CO_2$ is typically determined by using measurements from regions free from anthropogenic influence [40]. In this study, this quantification was performed by adopting measurements from desert localities in the western United States as representative background levels. The calculation formula is as follows:

$$C_{adj} = C_{obs} - C_{bg} \quad (1)$$

where $C_{adj}$ is the adjusted concentration, $C_{obs}$ is the observed concentration, and $C_{bg}$ is the background concentration. Only positive values, indicating net carbon emissions, were retained. Finally, we calculated the annual mean of these values for each state, which provided a representation of that state's emission level for the year. The formula for this final step is:

$$E = avg\left(C_{adj}^{+}\right) \quad (2)$$

where $avg(C_{adj}^{+})$ is the average function applied to all positive values of the adjusted concentration ($C_{adj}$). The value of E is then considered as the state-specific emission levels, represented as $\Delta CO$ and $\Delta XCO_2$. In this work, the calculated values of $\Delta CO$ and $\Delta XCO_2$ serve as proxies, to a certain extent, for the actual emissions of CO and $CO_2$, offering a more nuanced understanding of the anthropogenic impact on atmospheric gas concentrations.

### *4.1. Correlation Analysis*

#### 4.1.1. $NO_2$ and $CO_2$

To investigate the synergistic emission patterns of $NO_2$ and $CO_2$ emissions, we conducted a correlation analysis between the annual mean $\Delta NO_2$ and $\Delta XCO_2$ in ten states over the period spanning from 2019 to 2022, as depicted in Figure 7a.

Figure 7a illustrates a marked positive correlation (r = 0.75) between the annual mean $\Delta NO_2$ and $\Delta XCO_2$ in 10 states over the period of 2019–2022. This notable positive correlation suggests that states that exhibit elevated $NO_2$ emissions are associated with increased $CO_2$ emissions. The rationale for this linkage stems from the fact that $NO_2$ emissions are primarily a byproduct of fossil fuel combustion, a process concurrently responsible for the emission of $CO_2$.

Because $\Delta NO_2$ is numerically equivalent to the $NO_2$ concentration, the significant correlation between $NO_2$ and $CO_2$ emissions can also be extended to the relationship between the $NO_2$ concentration and $CO_2$ emissions. Owing to the extended atmospheric lifetime of $CO_2$ and its high atmospheric background levels, variations in $CO_2$ emissions are often indiscernible in observed $CO_2$ concentrations, which poses challenges for effective policy-making and the assessment of emission reduction efforts. Consequently, we can consider utilizing $NO_2$ as an indicator for $CO_2$ emissions due to $NO_2$'s shorter lifespan and its robust correlation with $CO_2$ emissions. To quantify the indicative role of $NO_2$

concentration on $CO_2$ emissions, we conducted a regression analysis between standardized $NO_2$ concentrations and $CO_2$ emissions. The standardization, often referred to as Z-score normalization, is mathematically represented as:

$$z = \frac{(X - \mu)}{\sigma} \quad (3)$$

where X is the original value, μ is the mean of the dataset, and σ is the standard deviation. This approach scales the data to have a mean of zero and a standard deviation of one. Based on standardized values, quantitatively, a 1% increase in $NO_2$ concentration corresponds to a 0.8194% (±0.0942%) rise in annual mean $CO_2$ emissions, as illustrated in Figure 7b.

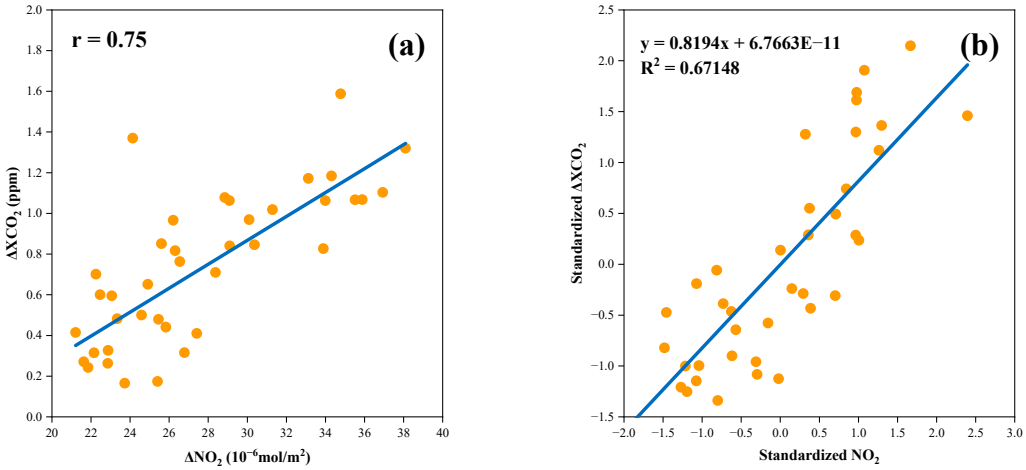


**Figure 7.** (**a**) Correlation between the annual mean $\Delta NO_2$ and $\Delta XCO_2$ in 10 states from 2019–2022. Each point represents the annual mean value for a single state, with $\Delta NO_2$ plotted on the *X*-axis and $\Delta XCO_2$ plotted on the *Y*-axis. (**b**) Regression analysis between standardized $NO_2$ concentration and standardized $\Delta XCO_2$.

#### 4.1.2. CO and $CO_2$, CO and $NO_2$

This study investigated the correlations between CO and $CO_2$ emissions, as well as CO and $NO_2$ emissions, over the period of 2019–2022, as depicted in Figure 8.

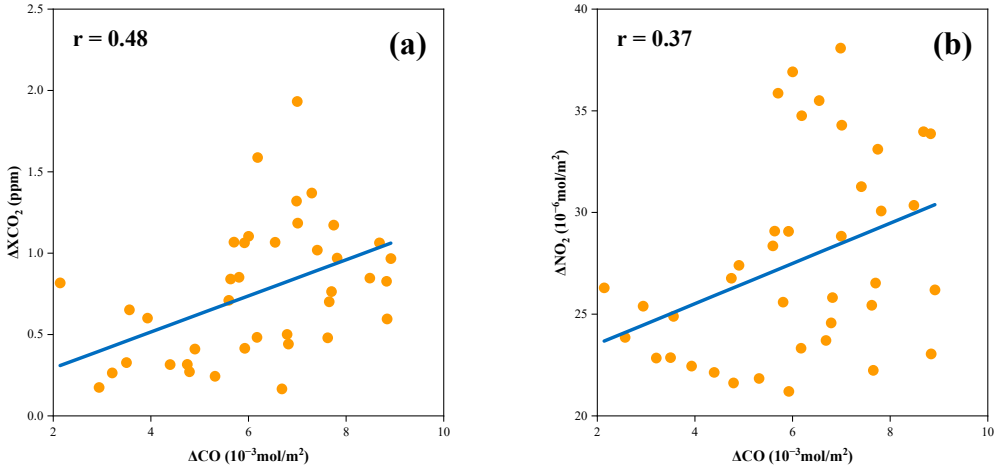


**Figure 8.** (**a**) Correlation between annual mean ΔCO and $\Delta XCO_2$ in 10 states from 2019-2022. Each point represents the annual mean value for a single state, with ΔCO plotted on the *X*-axis and $\Delta XCO_2$ plotted on the *Y*-axis. (**b**) Same as in Figure 8a but for annual mean ΔCO and $\Delta NO_2$.

Figure 8a shows a moderate linear correlation (r = 0.48) between $\Delta XCO_2$ and ΔCO, suggesting a modest associative relationship. This correlation is less pronounced as compared

to the correlation observed between the $\Delta XCO_2$ concentration and the $NO_2$ concentration. This correlation suggests that while both CO and $CO_2$ emissions share common sources and environmental influences, their emission dynamics are distinct in several aspects. Both CO and $CO_2$ are byproducts of combustion processes and are commonly emitted from sources like vehicles, industrial activities, and the burning of fuels. However, they differ in their impacts and the processes that lead to their formations. A considerable portion of human-induced $CO_2$ emissions originate from burning fossil fuels, whereas incomplete combustion from sources such as vehicle exhaust and forest fires creates the majority of CO emissions.

In Figure 8b, the correlation analysis highlights a notably weak link (r = 0.37) between CO and $NO_2$ emissions compared to other gas emissions studied. This minimal correlation can be primarily attributed to the differences in their emission sources. CO is primarily produced from incomplete combustion processes, such as those found in motor vehicles and industrial activities, whereas $NO_2$ is typically a byproduct of high-temperature combustion processes, such as power plants and vehicular engines, especially those that run on diesel.

### *4.2. Enhancement Ratio*

Given the different magnitudes of the observed concentration data for OCO-2 and TROPOMI, the data were normalized before emission ratios were calculated, thus enabling the obtainment of the enhancement ratios among $\Delta NO_2$, $\Delta CO$, and $\Delta XCO_2$. For clarity and simplicity in our presentation, the terms $\Delta NO_2$: $\Delta XCO_2$ and $\Delta CO$: $\Delta XCO_2$, as used in the subsequent sections of this paper, will exclusively denote the ratios obtained from normalized enhancement values.

#### 4.2.1. $\Delta NO_2$: $\Delta XCO_2$

Figure 9 presents the calculated $\Delta NO_2$: $\Delta XCO_2$ enhancement ratios for each of the 10 states.

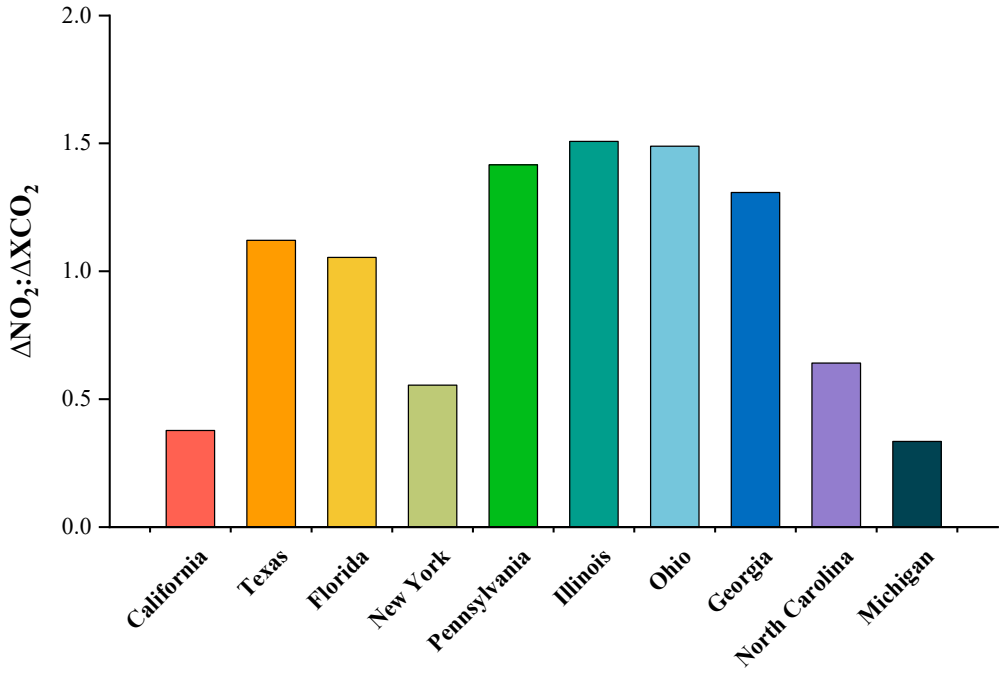


**Figure 9.** $\Delta NO_2$: $\Delta XCO_2$ derived by using observations from TROPOMI and OCO-2.

The $\Delta NO_2$: $\Delta XCO_2$ enhancement ratio is a widely used metric for describing the $NO_2$ pollution index per unit of $CO_2$ emitted. High emission ratios are generally associated with high $NO_2$ emissions and decreased combustion efficiencies. The variations observed in this enhancement ratio are dependent on several factors, including the type of combustion

equipment and the employed combustion technology. Of the 10 states examined, Illinois, Ohio, and Pennsylvania, which all have major manufacturing industries, have the highest emission ratios. The manufacturing industry has lower combustion emission efficacy than other industries because of its high dependence on fossil fuels and outdated production technology and equipment. As a result, Florida, wherein the main industry is tourism; New York, wherein the main industry is finance; and North Carolina, wherein the main industry is technology, all outperform other states in terms of combustion efficacy. However, Michigan, another automobile manufacturing hub, has a low emission ratio primarily due to its gradual shift away from high-pollution energy sources and toward clean alternatives, such as natural gas, wind, and solar energy. Furthermore, recent technological advancements, such as hybrid and battery-powered vehicles, have considerably reduced energy consumption and $NO_2$ emissions by automobile production. Similarly, M. Reuter et al. observed in the Middle East a correlation between the recently installed and renewed technology and a reduced emission ratio of nitrogen oxides ($NO_x$) and $CO_2$ [41].

#### 4.2.2. ΔCO: $\Delta XCO_2$

Figure 10 presents the calculated ΔCO: $\Delta XCO_2$ enhancement ratios for each of the 10 states.

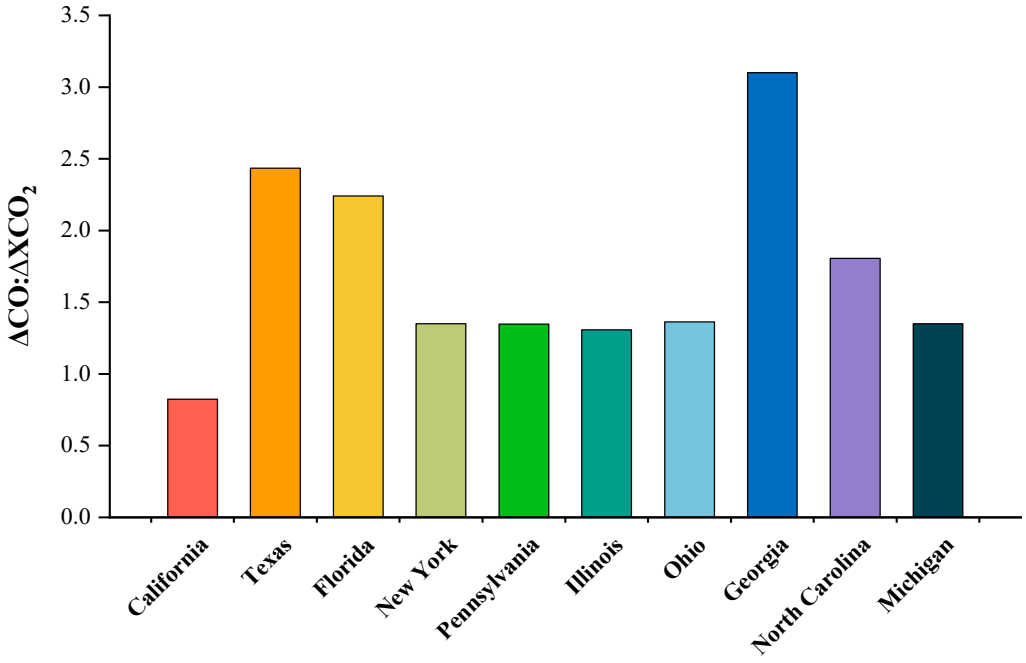


**Figure 10.** ΔCO: $\Delta XCO_2$ derived by using observations from TROPOMI and OCO-2.

The ΔCO: $\Delta XCO_2$ enhancement ratio serves as an index of regional combustion efficiency, with elevated ratios denoting increased levels of CO pollution per unit $CO_2$ emitted. Given that CO is indicative of incomplete combustion, a high enhancement ratio suggests diminished combustion efficiency. In the context of CO emissions, traditional fossil fuels are predisposed to generate higher quantities of CO—particularly under suboptimal combustion conditions—than clean energy alternatives. Indeed, certain clean energy modalities, such as solar and wind power, inherently eschew CO emissions owing to their lack of dependence on combustion processes, thereby exhibiting inherently superior combustion efficiency relative to conventional energy sources. This disparity is manifested in the emission ratios computed in this investigation. Compared with other states, Florida, Georgia, and Texas exhibit more pronounced emission ratios that are concomitant with their relatively modest adoption of clean energy, which accounted for 18.1%, 38.4%, and 33% of their energy portfolios in 2021, respectively. Conversely, California and Illinois, which have lower emission ratios than other states, have embraced clean energy to the extent of

50.7% and 64.5% of their overall energy consumption, respectively. This observation aligns with findings of Hayoung Park et al., who identified that elevated CO: $CO_2$ emission ratios can be attributed to the low combustion efficiency of fossil fuels. Similarly, the use of the clean energy sources mentioned above serves as a replacement for fossil fuels and likewise demonstrates the relationship between emission ratios and combustion efficiency [42].

## 5. Discussion

In our investigation, we comprehensively examined the seasonal variations of $NO_2$, CO, and $CO_2$ concentrations and their interrelationships emissions across the 10 most populous states in the United States, culminating in the derivation of state-specific $\Delta NO_2$: $\Delta XCO_2$ and $\Delta CO$: $\Delta XCO_2$ emission ratios.

In analyzing the concentration trends of $NO_2$ and CO, we observed the notable impact of the COVID-19 pandemic on these atmospheric pollutants [43]. During the spring of 2020, which marked the peak of stringent lockdown measures, the $NO_2$ concentrations in these states showed a universal decline as compared to the spring of 2019. It is noteworthy that this phenomenon is not an exception on a global scale. For instance, Akash Biswal et al. (2021) reported a decrease of 20–40% in $NO_2$ concentrations in urban clusters in India during their lockdown period. Similarly, Maria-Elissavet Koukouli et al. observed an average reduction of 11% and 15% in $NO_2$ levels in six major Greek urban areas in March and April 2021, respectively [44]. Matthew J. Cooper et al. found a more pronounced average reduction of 28.7% ($\pm$14.6%) in $NO_2$ levels between 2019 and 2020 (peak lockdown period) across various U.S. cities [45]. This reduction was higher than what was calculated in our study. Therefore, more expansive research is warranted in order to provide a more comprehensive understanding. Regarding the observation of CO concentration trends, a marked shift was noted in the aftermath of the COVID-19 pandemic, characterized by a trend toward stabilization and a general downward trajectory. This phenomenon is consistent with global observations, as delineated in the work by Hamideh Habibi et al., underscoring the pandemic's significant environmental impact [46]. Intriguingly, our analysis also revealed an aberration in the seasonal patterns of CO concentrations in certain locales during the autumn and winter months, which notably dissipated following the pandemic's subsidence in 2022. This deviation from established seasonal norms underscores the profound influence of human activity on atmospheric gas concentrations, thereby accentuating our collective responsibility in steering toward improved atmospheric conditions.

Additionally, our study probed into the co-emission characteristics of these gases, with particular emphasis on the role of $NO_2$ as a potential precursor of $CO_2$ emissions. This aspect resonates with the findings in the acclaimed study by Gerrit Kuhlmann et al. In their study, $NO_2$ is introduced into the quantification of $CO_2$ emissions from power plants. The observed correlations between the emissions of these gases not only reflect their inherent emission dynamics but also illuminate the prospects for synergistic mitigation strategies [47]. By concentrating on common emission sources, we can forge targeted approaches in environmental policy-making, addressing key sectors such as fuel consumption in transportation ($CO_2$ and CO), vehicular control and technological advancement ($NO_2$ and CO), and industrial process optimization ($NO_2$ and $CO_2$). Nevertheless, such policy frameworks must judiciously balance environmental objectives with the economic feasibility, specific energy, and resource landscapes of each state.

In the final facet of our analysis, we evaluated the emission ratios across these states. The $\Delta NO_2$: $\Delta XCO_2$ enhancement ratio, in particular, seems to be intricately linked with the industrial fabrics of the states, manufacturing states exhibiting higher ratios than those dominated by high-tech industries. A notable exception was Michigan, a state synonymous with automotive manufacturing, which demonstrated a lower emission ratio, indicative of higher combustion efficiency. This observation challenges the traditional paradigm linking manufacturing with lower combustion efficiency and higher emissions, suggesting alternative pathways for emission optimization that do not necessitate industrial paradigm

shifts. Such approaches could potentially offer cost-effective solutions, considering the inherent risks and expenses associated with transitioning to new industrial sectors. The $\Delta CO$: $\Delta XCO_2$ enhancement ratio, correlated with predominant fuel types, emerged as a potential indicator of urban environmental quality and production efficiency, where higher ratios may imply lower combustion efficiency and increased pollutant output. For states exhibiting elevated $\Delta CO$: $\Delta XCO_2$ enhancement ratios, it would be beneficial to explore opportunities to enhance combustion efficiency through the thoughtful modification of fuel types. In addressing the complexities of emission characteristic analyses, it is critical to acknowledge the uncertainties within our calculated enhancement ratios, such as spatial and temporal heterogeneity within state-level data. Given these considerations, the ratios presented in this study should be interpreted with caution. While these ratios provide insights into emission trends and patterns, they may not precisely mirror the exact emission proportions due to the aforementioned variabilities. Therefore, in interpreting these ratios, it is advisable to consider them as indicative rather than as definitive representations of state-specific emissions. Enhancing the reliability of data through more rigorous data selection and analytical methods will be a goal for future research.

Because this study primarily concentrates on the United States' most densely populated states, its broader applicability warrants further exploration. Future research expanding to a more diverse array of geographical contexts will be instrumental in enriching our understanding of the multifaceted impact of human activities on atmospheric dynamics.

## 6. Conclusions

This study demonstrates the seasonal variation characteristics of $CO_2$, CO, and $NO_2$ concentrations in the 10 most densely populated states in the United States from autumn 2018–winter 2020. The concentration pattern of $XCO_2$ displays a Z-shaped increase, peaking in the spring and dipping in the summer. Meanwhile, the magnitude of its decline during the summer is related to the forest coverage in each state. In regions characterized by extensive forest coverage, there is a notable tendency for a more pronounced decrease in $CO_2$ concentrations during the summer months. Similarly, atmospheric $NO_2$ levels are lower in summer and higher in winter, and are correlated with state-specific average winter temperatures and heating-related emissions. During the spring of 2020, which marked the zenith of lockdown measures, $NO_2$ concentration levels across the 10 states demonstrated reductions ranging from 1.27% to 22.25% in comparison to the corresponding period in the preceding year. CO concentrations, on the other hand, peak in spring and reach their nadir in summer, with the anomalously elevated CO levels observed during the summer months that are potentially indicative of wildfire incidents. Additionally, coastal, and natural gas-dominant areas exhibit low CO levels. The COVID-19 pandemic and associated containment measures exerted a pronounced influence on atmospheric CO concentrations. There was a marked flattening of the CO concentration trajectory, which was then followed by a general declining trend. In the winter of 2021, there was an exceptional reduction in CO concentrations, representing a deviation from the established seasonal norms. Despite a moderate rebound following the cessation of the epidemic, the elevations observed in the winter of 2022 persisted at levels that were notably lower than the baseline established prior to the pandemic.

Furthermore, we discussed the correlation between $CO_2$, $NO_2$, and CO emissions. Notably, the strongest correlation was observed between $NO_2$ and $CO_2$ emissions, with a correlation coefficient (r) of 0.75. This was followed by a correlation of 0.48 between $CO_2$ and CO emissions and a relatively weaker correlation of 0.37 between CO and $NO_2$ emissions. Given the relatively brief atmospheric lifespan of $NO_2$, its concentration levels can serve as a fairly accurate reflection of $NO_2$ emissions. Consequently, $NO_2$ concentration emerges as a reliable proxy for estimating $CO_2$ emissions. Our findings indicate that a 1% increase in $NO_2$ concentration is associated with a 0.8194% ($\pm$0.0942%) increase in the annual mean of $CO_2$ emissions.

Lastly, we calculated the enhancement ratios among CO, $NO_2$, and $XCO_2$. States with high $\Delta NO_2$: $\Delta XCO_2$ enhancement ratios have concentrations of industry types in the manufacturing sector. Meanwhile, the degree of the industrial sophistication of states with the same industry types is reflected by $\Delta NO_2$: $\Delta XCO_2$ enhancement ratios. High observed enhancement ratios tend to represent outdated industrial structures and production technologies. Accordingly, low $\Delta CO$: $\Delta XCO_2$ enhancement ratios are associated with states utilizing clean energy sources, thus highlighting the environmental benefits of such practices.

**Author Contributions:** The study was completed with cooperation between all authors. C.X. and A.X. designed the research topic; A.X. conducted the experiment; C.X. checked and analyzed the experimental results; C.X. and A.X. wrote the paper. All authors have read and agreed to the published version of the manuscript.

**Funding:** This research was funded in part by the Natural Science Foundation of Jiangsu Province, China under Grants BK20180809; in part by the National Natural Science Foundation of China under Grants 41901274; in part by the Talent Launch Fund of Nanjing University of Information Science and Technology under Grant 2017r066.

**Data Availability Statement:** This study makes use of data obtained from publicly accessible satellite sensors, detailed as follows: The $NO_2$ and CO concentration data derived from the Tropospheric Monitoring Instrument (TROPOMI) sensor are available in Google Earth Engine (GEE). For access to these datasets, please visit the following links: [Sentinel-5P TROPOMI NO2 Data Products] (https://developers.google.com/earth-engine/datasets/catalog/COPERNICUS_S5P_OFFL_L3_NO2 (accessed on 18 December 2023)). [Sentinel-5P TROPOMI CO Data Products] (https://developers.google.com/earth-engine/datasets/catalog/COPERNICUS_S5P_OFFL_L3_CO (accessed on 18 December 2023)). The column-averaged dry air mole fractions of CO2 (XCO2) data retrieved from the Orbiting Carbon Observatory-2 (OCO-2) satellite measurements are accessible through the Goddard Earth Sciences Data and Information Services Center (GES DISC). This data can be found here: https://disc.gsfc.nasa.gov/datasets/OCO2_L2_Lite_FP_11r/summary (accessed on 18 December 2023). Ground-truth measurements for $NO_2$ concentrations were sourced from the Environmental Protection Agency's (EPA) Air Quality System (AQS) monitoring network. This data can be found here: [EPA Outdoor Air Quality Data] (https://www.epa.gov/outdoor-air-quality-data (accessed on 18 December 2023)). As for the processed data underlying the final conclusions, it has been duly presented in the article. Should there be a need for any data from intermediate stages of processing, please reach out to the corresponding author.

**Acknowledgments:** We express our sincere appreciation to OCO-2, TROPOMI, and the Google Earth Engine (GEE) for their essential data contributions to this research. Our gratitude also goes to EPA, Wisevoter, the National Centers for Environmental Information, ycharts, the Nuclear Energy Institute, and the Bureau of Transportation Statistics for providing critical data, which were invaluable to our analysis.

**Conflicts of Interest:** The authors declare no conflict of interest.

## References

1. United Nations Environment Programme. 2021 Annual Report. Available online: https://www.unep.org/resources/annual-report-2021 (accessed on 20 October 2023).
2. Arias, P.A.; Bellouin, N.; Coppola, E.; Jones, R.G.; Krinner, G.; Marotzke, J.; Naik, V.; Palmer, M.D.; Plattner, G.-K.; Rogelj, J.; et al. 2021: Technical Summary. In *Climate Change 2021: The Physical Science Basis. Contribution of Working Group I to the Sixth Assessment Report of the Intergovernmental Panel on Climate Change*; Masson-Delmotte, V., Zhai, P., Pirani, A., Connors, S.L., Péan, C., Berger, S., Caud, N., Chen, Y., Goldfarb, L., Gomis, M.I., et al., Eds.; Cambridge University Press: Cambridge, UK; New York, NY, USA, 2021; pp. 33–144. [CrossRef]
3. Zhang, H.; Han, G.; Ma, X.; Chen, W.; Zhang, X.; Liu, J.; Gong, W. Robust algorithm for precise $XCO_2$ retrieval using single observation of IPDA LIDAR. *Opt. Express* **2023**, *31*, 11846–11863. [CrossRef]
4. Pei, Z.; Han, G.; Mao, H.; Chen, C.; Shi, T.; Yang, K.; Ma, X.; Gong, W. Improving quantification of methane point source emissions from imaging spectroscopy. *Remote Sens. Environ.* **2023**, *295*, 113652. [CrossRef]
5. Cai, M.; Han, G.; Ma, X.; Pei, Z.; Gong, W. Active–passive collaborative approach for $XCO_2$ retrieval using spaceborne sensors. *Opt. Lett.* **2022**, *47*, 4211–4214. [CrossRef]

6. Jones, M.W.; Peters, G.P.; Gasser, T.; Andrew, R.M.; Schwingshackl, C.; Gütschow, J.; Houghton, R.A.; Friedlingstein, P.; Pongratz, J.; Le Quéré, C. National Contributions to Climate Change Due to Historical Emissions of Carbon Dioxide, Methane, and Nitrous Oxide Since 1850. *Sci. Data* **2023**, *10*, 155. [CrossRef] [PubMed]
7. Watson, D. How Exactly Does Carbon Dioxide Cause Global Warming? Columbia Climate School. 2023. Available online: https://news.climate.columbia.edu (accessed on 14 November 2023).
8. Sellers, P.J.; Bounoua, L.; Collatz, G.J.; Randall, D.A.; Dazlich, D.A.; Los, S.O.; Berry, J.A.; Fung, I.; Tucker, C.J.; Field, C.B.; et al. Comparison of Radiative and Physiological Effects of Doubled Atmospheric $CO_2$ on Climate. *Science* **1996**, *271*, 1402–1406. [CrossRef]
9. Shi, T.; Han, G.; Ma, X.; Pei, Z.; Chen, W.; Liu, J.; Zhang, X.; Li, S.; Gong, W. Quantifying strong point sources emissions of $CO_2$ using spaceborne LiDAR: Method development and potential analysis. *Energy Convers. Manag.* **2023**, *292*, 117346. [CrossRef]
10. Qiu, R.; Han, G.; Li, S.; Tian, F.; Ma, X.; Gong, W. Soil moisture dominates the variation of gross primary productivity during hot drought in drylands. *Sci. Total Environ.* **2023**, *899*, 165686. [CrossRef] [PubMed]
11. Pei, Z.; Han, G.; Shi, T.; Ma, X.; Gong, W. A $XCO_2$ Retrieval Algorithm Coupled Spatial Correlation for the Aerosol and Carbon Detection Lidar. *Atmos. Environ.* **2023**, *309*, 119933. [CrossRef]
12. Gorman, D.; Drewry, A.; Huang, Y.L.; Sames, C. The Clinical Toxicology of Carbon Monoxide. *Toxicology* **2003**, *187*, 25–38. [CrossRef]
13. Kawaragi, K.; Sekine, Y.; Kadono, T.; Sugita, S.; Ohno, S.; Ishibashi, K.; Kurosawa, K.; Matsui, T.; Ikeda, S. Direct Measurements of Chemical Composition of Shock-Induced Gases from Calcite: An Intense Global Warming After the Chicxulub Impact Due to the Indirect Greenhouse Effect of Carbon Monoxide. *Earth Planet. Sci. Lett.* **2009**, *282*, 56–64. [CrossRef]
14. Bai, L.; Shin, S.; Burnett, R.T.; Kwong, J.C.; Hystad, P.; van Donkelaar, A.; Goldberg, M.S.; Lavigne, E.; Weichenthal, S.; Martin, R.V.; et al. Exposure to Ambient Air Pollution and the Incidence of Lung Cancer and Breast Cancer in the Ontario Population Health and Environment Cohort. *Int. J. Cancer* **2020**, *146*, 2450–2459. [CrossRef] [PubMed]
15. Khomenko, S.; Cirach, M.; Pereira-Barboza, E.; Mueller, N.; Barrera-Gómez, J.; Rojas-Rueda, D.; de Hoogh, K.; Hoek, G.; Nieuwenhuijsen, M. Premature Mortality Due to Air Pollution in European Cities: A Health Impact Assessment. *Lancet Planet. Health* **2021**, *5*, e121–e134. [CrossRef] [PubMed]
16. Koenig, J.Q. Air Pollution and Asthma. *J. Allergy Clin. Immunol.* **1999**, *104*, 717–722. [CrossRef] [PubMed]
17. Kuhlmann, G.; Henne, S.; Meijer, Y.; Brunner, D. Quantifying $CO_2$ Emissions of Power Plants with $CO_2$ and $NO_2$ Imaging Satellites. *Front. Remote Sens.* **2021**, *2*, 14.
18. Paraschiv, S.; Barbuta-Misu, N.; Paraschiv, S.L. Influence of $NO_2$, NO and Meteorological Conditions on the Tropospheric $O_3$ Concentration at an Industrial Station. *Energy Rep.* **2020**, *6*, 231–236. [CrossRef]
19. Lama, S.; Houweling, S.; Boersma, K.F.; Eskes, H.; Aben, I.; Denier van der Gon, H.A.C.; Krol, M.C.; Dolman, H.; Borsdorff, T.; Lorente, A. Quantifying burning efficiency in megacities using the $NO_2$/CO ratio from the Tropospheric Monitoring Instrument (TROPOMI). Atmos. *Chem. Phys.* **2020**, *20*, 10295–10310. [CrossRef]
20. MacDonald, C.G.; Mastrogiacomo, J.-P.; Laughner, J.L.; Hedelius, J.K.; Nassar, R.; Wunch, D. Estimating enhancement ratios of nitrogen dioxide, carbon monoxide, and carbon dioxide using satellite observations. *Atmos. Chem. Phys.* **2023**, *23*, 3493–3516. [CrossRef]
21. Wan, N.; Xiong, X.; Kluitenberg, G.J.; Hutchinson, J.M.S.; Aiken, R.; Zhao, H.; Lin, X. Estimation of biomass burning emission of $NO_2$ and CO from 2019–2020 Australia fires based on satellite observations. *Atmos. Chem. Phys.* **2023**, *23*, 711–724. [CrossRef]
22. Ritchie, H.; Roser, M.; Rosado, P. $CO_2$ and Greenhouse Gas Emissions. Our World in Data. 2020. Available online: https://ourworldindata.org/co2-and-greenhouse-gas-emissions (accessed on 5 September 2023).
23. Qiu, R.; Li, X.; Han, G.; Xiao, J.; Ma, X.; Gong, W. Monitoring drought impacts on crop productivity of the US Midwest with solar-induced fluorescence: GOSIF outperforms GOME-2 SIF and MODIS NDVI, EVI, and NIRv. *Agric. For. Meteorol.* **2022**, *323*, 109038. [CrossRef]
24. Sentinel-5P TROPOMI $NO_2$ Data Products. Available online: https://developers.google.com/earth-engine/datasets/catalog/COPERNICUS_S5P_OFFL_L3_NO2 (accessed on 10 March 2023).
25. Sentinel-5P TROPOMI CO Data Products. Available online: https://developers.google.com/earth-engine/datasets/catalog/COPERNICUS_S5P_OFFL_L3_CO (accessed on 10 March 2023).
26. OCO-2/OCO-3 Science Team; Payne, V.; Chatterjee, A. *OCO-2 Level 2 Bias-Corrected XCO2 and Other Select Fields from the Full-Physics Retrieval Ag-gregated as Daily Files, Retrospective Processing V11r*; GES DISC: Greenbelt, MD, USA, 2020. Available online: https://disc.gsfc.nasa.gov/datasets/OCO2_L2_Lite_FP_11r/summary (accessed on 25 March 2023).
27. Zhou, S.; Collier, S.; Jaffe, D.A.; Zhang, Q. Free Tropospheric Aerosols at the Mt. Bachelor Observatory: More Oxidized High. Sulfate Content Comp. Bound. Layer Aerosols. *Atmos. Chem. Phys.* **2019**, *19*, 1571–1585. [CrossRef]
28. Veefkind, J.P.; Aben, I.; McMullan, K.; Förster, H.; De Vries, J.; Otter, G.; Claas, J.; Ekses, H.J.; de Haan, J.F.; Keipool, Q.; et al. TROPOMI on the ESA Sentinel-5 Precursor: A GMES Mission for Global Observations of the Atmospheric Composition for Climate, Air Quality, and Ozone Layer Applications. *Remote Sens. Environ.* **2012**, *120*, 70–83. [CrossRef]
29. Kiel, M.; Das, S.; Osterman, G.; Laughner, J.; Payne, V.; Chatterjee, A. Evaluation of the OCO-2 and OCO-3 ACOS Data Products Against TCCON. In Proceedings of the EGU General Assembly Conference Abstracts, Vienna, Austria, 23–28 April 2023. EGU-10615.
30. Olivier, J.G.J.; Schure, K.M.; Peters, J. Trends in Global $CO_2$ and Total Greenhouse Gas Emissions. *PBL Neth. Environ. Assess. Agency* **2017**, *5*, 1–11.

31. Dean, A. Deforestation and Climate Change. Climate Council. Available online: https://www.climatecouncil.org.au (accessed on 21 October 2023).
32. Griffin, K.L.; Seemann, J.R. Plants, $CO_2$ and Photosynthesis in the 21st Century. *Chem. Biol.* **1996**, *3*, 245–254. [CrossRef] [PubMed]
33. Moore, C.E.; Meacham-Hensold, K.; Lemonnier, P.; Slattery, R.A.; Benjamin, C.; Bernacchi, C.J.; Lawson, T.; Cavanagh, A.P. The Effect of Increasing Temperature on Crop Photosynthesis: From Enzymes to Ecosystems. *J. Exp. Bot.* **2021**, *72*, 2822–2844. [CrossRef] [PubMed]
34. Chen, X.; Ren, X.; He, H.; Zhang, L.; Lv, Y. Seasonal Variation of Ecosystem Photosynthetic Capacity and Its Environmental Drivers in Global Grasslands. *Front. Ecol. Evol.* **2023**, *11*, 1193607. [CrossRef]
35. Van Der, A.R.J.; Eskes, H.J.; Boersma, K.F.; Van Noije TP, C.; Van Roozendael, M.; De Smedt, I.; Peters, D.H.M.U.; Meijer, E.W. Trends, Seasonal Variability and Dominant NOx Source Derived from a Ten Year Record of $NO_2$ Measured from Space. *J. Geophys. Res. Atmos.* **2008**, *113*. [CrossRef]
36. Plaisance, H.; Piechocki-Minguy, A.; Garcia-Fouque, S.; Galloo, J.C. Influence of Meteorological Factors on the $NO_2$ Measurements by Passive Diffusion Tube. *Atmos. Environ.* **2004**, *38*, 573–580. [CrossRef]
37. Van Dop, H.; Krol, M. Changing Trends in Tropospheric Methane and Carbon Monoxide: A Sensitivity Analysis of the OH-Radical. *J. Atmos. Chem.* **1996**, *25*, 271–288. [CrossRef]
38. Holloway, T.; Levy, H.; Kasibhatla, P. Global Distribution of Carbon Monoxide. *J. Geophys. Res. Atmos.* **2000**, *105*, 12123–12147. [CrossRef]
39. Loehman, R.A. Drivers of Wildfire Carbon Emissions. *Nat. Clim. Chang.* **2020**, *10*, 1070–1071. [CrossRef]
40. Pei, Z.; Han, G.; Ma, X.; Shi, T.; Gong, W. A Method for Estimating the Background Column Concentration of $CO_2$ Using the Lagrangian Approach. *Ieee Trans. Geosci. Remote Sens.* **2022**, *60*, 1–12.
41. Reuter, M.; Buchwitz, M.; Hilboll, A.; Richter, A.; Schneising, O.; Hilker, M.; Heymann, J.; Bovensmann, H.; Burrows, J.P. Decreasing emissions of NOx relative to $CO_2$ in East Asia inferred from satellite observations. *Nat. Geosci.* **2014**, *7*, 792–795. [CrossRef]
42. Park, H.; Jeong, S.; Park, H.; Labzovskii, L.D.; Bowman, K.W. An assessment of emission characteristics of Northern Hemisphere cities using spaceborne observations of $CO_2$, CO, and $NO_2$. *Remote Sens. Environ.* **2021**, *254*, 112246. [CrossRef]
43. Pei, Z.; Han, G.; Ma, X.; Su, H.; Gong, W. Response of major air pollutants to COVID-19 lockdowns in China. *Sci. Total Environ.* **2020**, *743*, 140879. [CrossRef] [PubMed]
44. Koukouli, M.-E.; Skoulidou, I.; Karavias, A.; Parcharidis, I.; Balis, D.; Manders, A.; Segers, A.; Eskes, H.; van Geffen, J. Sudden changes in nitrogen dioxide emissions over Greece due to lockdown after the outbreak of COVID-19. Atmos. *Chem. Phys.* **2021**, *21*, 1759–1774. [CrossRef]
45. Poetzscher, J.; Isaifan, R.J. The impact of COVID-19-induced lockdowns during spring 2020 on nitrogen dioxide levels over major American counties. *Elem. Sci. Anth.* **2021**, *9*, 00002. [CrossRef]
46. Habibi, H.; Awal, R.; Fares, A.; Ghahremannejad, M. COVID-19 and the Improvement of the Global Air Quality: The Bright Side of a Pandemic. *Atmosphere* **2020**, *11*, 1279. [CrossRef]
47. Shi, T.; Han, G.; Ma, X.; Mao, H.; Chen, C.; Han, Z.; Pei, Z.; Zhang, H.; Li, S.; Gong, W. Quantifying factory-scale $CO_2/CH_4$ emission based on mobile measurements and EMISSION-PARTITION model: Cases in China. *Environ. Res. Lett.* **2023**, *18*, 034028. [CrossRef]


**Disclaimer/Publisher's Note:** The statements, opinions and data contained in all publications are solely those of the individual author(s) and contributor(s) and not of MDPI and/or the editor(s). MDPI and/or the editor(s) disclaim responsibility for any injury to people or property resulting from any ideas, methods, instructions or products referred to in the content.